Inorganic Chemistry

ARTICLE

pubs.acs.org/IC

# Facile Synthesis of ZnS−$CuInS_2$-Alloyed Nanocrystals for a Color-Tunable Fluorchrome and Photocatalyst

Wenjin Zhang and Xinhua Zhong*

Key Laboratory for Advanced Materials, Department of Chemistry, East China University of Science and Technology, Shanghai 200237, China

Supporting Information

**ABSTRACT:** High-quality ZnS−$CuInS_2$ (ZCIS) alloy nanocrystals have been synthesized via reaction between the acetate salts of the corresponding metals and elemental sulfur in the presence of dodecanethiol in octadecene media at 230 °C. The PL emission wavelength can be tuned conveniently via variation of the stoichiometric ratio of their components. The influence of various experimental variables, including Zn/CuIn ratio, amount of sulfur and dodecanethiol, and reaction temperature, on the optical properties and composition of the obtained ZCIS NCs have been systematically investigated. The plain ZCIS NCs did show PL emission but with quite low PL quantum yield (typically below 3%). In order to improve the PL emission efficiency, the ZnS shell was subsequently overcoated around the ZCIS core NCs. With ZnS shell growth, the PL emission wavelength of the resulting ZCIS/ZnS NCs can cover from 518 to 810 nm with the maximum PL quantum efficiency up to 56%. Furthermore, the obtained ZCIS/ZnS NCs show promising photocatalytic activity in the degradation of rhodamine B.

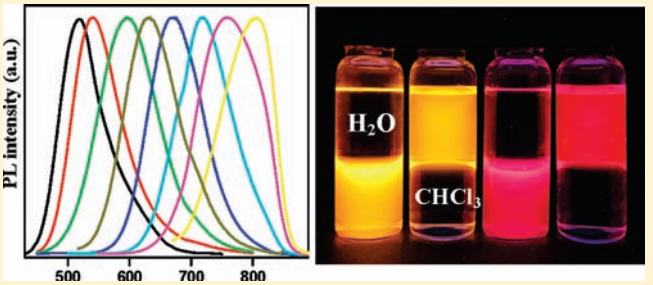


## INTRODUCTION

Semiconductor nanocrystals (NCs) with tunable band gaps are attractive materials for various applications, such as light-emitting diodes, solar cells, biolabeling, etc.[1−6] In general, the band gap of semiconductor NCs can be tuned by varying the particle size due to the quantum size effect or by tuning constituent stoichiometries in alloyed NCs. However, tuning the band gap by simply adjusting the particle size would limit in extending the emission range and achieving a narrow range of fluorescence colors since unstable small particles or large particles with a size greater than the exciton Bohr radius are not favorable for the emission efficiency. In addition, the size-dependent properties will disappear once the NCs are deposited onto thin film and undergone the thermal process for different applications. In contrast, composition control is a more feasible route to fabricate semiconductor thin films with tunable band gaps. Furthermore, different band gaps can be conveniently achieved through variation of the composition in multicomponent NCs even under a fixed size. For these reasons, a great variety of alloyed NCs, such as $Zn_xCd_{1-x}Se$,[7,8] $Zn_xCd_{1-x}S$,[9,10] $CuIn_xGa_{1-x}S_2$,[11,12] $CuGa_xIn_{1-x}Se_2$,[4,13,14] $AgInS_2$−ZnS,[15−17] and $CuInS_2$−ZnS,[18−20] have been extensively investigated. Despite II−VI and IV−VI semiconductor NCs possessing appealing optical properties, the intrinsic toxicity of cadmium and lead sheds doubt on the future applicability of these NCs, particularly in view of recent environmental regulations.

Recently, chalcopyrite semiconductors $CuInS_2$ (CIS) and their alloyed nanocrystals with different materials of I−III−VI or II−VI semiconductors have been intensively investigated,[18−33] because these particles are direct band-gap semiconductors having a large absorption coefficient and containing no highly toxic elements. Alloying CIS ($E_g$ = 1.5 eV) with ZnS ($E_g$ = 3.7 eV) can create a family of NCs with band gaps covering almost the whole visible spectrum, which is of special interest in both solar energy conversion and fluorescence emitters. An early example of alloying CIS with ZnS was reported by Nakamura and co-workers through the thermolysis of zinc dithiocarbamate with the copper and indium iodide in oleylamine solution.[18] The obtained $CuInS_2$−ZnS (ZCIS)-alloyed NCs with PL wavelength controllable within 570−800 nm. Later, Pan et al. synthesized ZCIS NCs through thermolysis of coprecursors (Zn, Cu, and In complexes of diethyldithiocarbamate) in the presence of capping agent (oleic acid or dodecanethiol) and activation agent (oleylamine) and tuned the band gap of ZCIS NCs in a broad range covering almost the whole visible spectrum by changing the ratio of CIS to ZnS, but no luminescent properties were reported.[19] Very recently, Wang et al. developed a general method for the synthesis of a series of Cu−In−S-based multicomponent solid−solution NCs by a simple solvothermal process using metal diethyldithiocarbamate complexes as the precursors.[20]

Due to the promising properties of ZCIS, herein we intended to explore controlled synthesis of ZCIS-alloyed NCs using a "greener" approach and tuning their PL emission wavelength via variation of the stoichiometric ratio of their components. ZCIS-alloyed NCs were prepared in a noncoordinating solvent

**Received:** December 23, 2010
**Published:** April 01, 2011

octadecene using acetate salts of copper, indium, and zinc as their precursors. The key for successful synthesis of the nearly monodisperse ZCIS NCs was to balance the reactivity of the three cationic precursors with the use of proper capping reagents (dodecanethiol). The plain ZCIS NCs did show PL emission but with quite low PL quantum yield, typically below 3%. In order to improve the PL emission efficiency, ZnS shell was subsequently deposited around the ZCIS core NCs. With the shell growth, the PL QY increased substantially with the maximum value of 56% and emission wavelength tunable from 518 to 810 nm. The high PL emission efficiency of the ZCIS/ZnS NCs can also be preserved after phase transfer via ligand replacement. Besides the excellent optical properties, the obtained ZCIS/ZnS NCs also exhibit promising photocatalytic activity in the degradation of rhodamine B.

## EXPERIMENTAL SECTION

**Chemicals.** Copper acetate ($Cu(OAc)_2$, 99.99%), indium acetate ($In(OAc)_3$, 99.99%), zinc acetate ($Zn(OAc)_2$, 99.99%), sulfur powder (99.99%), dodecanethiol (DDT, 99.9%), stearic acid (SA, 95%), octadecylamine (OAm, 97%), 1-octadecene (ODE, 90%), 11-mercaptoundecanoic acid (MUA, 95%), rhodamine B (RhB), and tetramethylammonium hydroxide (TMAH, 97%) were purchased from Aldrich. All chemicals were used without further purification.

**Stock Solutions Preparation.** A 0.399 g (2 mmol) amount of $Cu(OAc)_2$, 1.137 g (4.0 mmol) of SA, and 9.0 mL of ODE were loaded in a three-neck flask clamped in a heating mantle. The mixture was heated to 160 °C under argon flow and remained at this temperature for about 10 min until formation of a clear deep green solution. The obtained Cu stock solution (0.2 M) was stored at 50 °C for following use.

A 0.584 g (2 mmol) amount of $In(OAc)_3$, 2.274 g (8.0 mmol) of SA, and 8.0 mL of ODE were loaded in a three-neck flask clamped in a heating mantle. The mixture was heated to 200 °C under argon flow and remained at this temperature for about 10 min until formation of a clear colorless solution. The obtained In stock solution (0.2 M) was stored at 50 °C for following use.

A 1.756 g (8 mmol) amount of $Zn(OAc)_2$, 6.0 mL of OAm, and 14.0 mL of ODE were loaded in a three-neck flask clamped in a heating mantle. The mixture was heated to 160 °C under argon flow and remained at this temperature for about 10 min until formation of a clear colorless solution. The obtained Zn stock solution (0.4 M) was stored at 50 °C for following use.

**Synthesis of ZCIS Core and ZCIS/ZnS NCs.** In a typical procedure, 1.0 mL of Cu stock solution (0.2 mmol), 1.0 mL of In stock solution (0.2 mmol), 0.25 mL of Zn stock solution (0.1 mmol), 1.0 mL of DDT, and 3.0 mL of ODE were loaded in a 50-mL three-neck flask clamped in a heating mantle. The mixture was heated to 230 °C under argon flow. Then 0.8 mL of ODE-S solution (0.32 mmol), obtained by dissolving 4.0 mmol of sulfur in 10.0 mL of ODE at 120 °C, was injected into the reaction system and kept at this temperature to allow growth of ZCIS NCs. Aliquots of the sample were taken at different time intervals and injected into cold toluene to terminate growth of NCs immediately for use of recording their optical spectra. After completion of particle growth, the reaction mixture was allowed to cool to 60 °C, and 10 mL of toluene was added thereafter. The obtained ZCIS NCs were precipitated by adding methanol into the toluene solution and purified by repeated centrifugation and decantation.

Deposition of ZnS shell around the ZCIS core template started when the ZCIS core grew at 230 °C for 30 min. The reaction temperature was raised to 240 °C for the following overgrowth of the ZnS shell. A 3 mL amount of Zn stock solution was injected into the reaction mixture in 5 batches with a time interval of 15 min. To monitor the reaction, aliquots were taken before injection of a new batch of Zn stock and their corresponding optical spectra were recorded accordingly. Purification of ZCIS/ZnS NCs was similar to that of ZCIS NCs.

**Water Solubilization of Oil-Soluble QDs via Ligand Replacement.** Water solubilization of the initially oil-soluble ZCIS/ZnS NCs was achieved by replacing the initial hydrophobic surfactants (DDT and/or stearate) with hydrophilic thiol ligand (MUA) according to the literature method.[34] Typically, MUA (0.5 g) was dissolved in 5.0 mL of methanol and the pH of the solution was adjusted to 9 with addition of TMAH. The MUA−methanol solution (0.5 mL) was then added into 5.0 mL of NCs toluene solution and stirred for 30 min at 70 °C to get precipitation of NCs. Then 5.0 mL of distilled water was added into the mixture and kept stirring for another 20 min. The solution was separated into two phases finally, and the NCs were transferred into the supernatant aqueous phase from the underlying toluene, which was discarded, and the aqueous phase containing the NCs was collected. The free MUA ligand in the NCs aqueous solution was isolated by precipitating the NCs with addition of acetone. The supernatant was discarded, and the pellet was then redissolved in water to get the purified NCs aqueous solution for further use.

**Characterization.** UV−vis and PL spectra were obtained on a Shimadzu UV-2450 UV−vis spectrophotometer and a Cary Eclipse (Varian) fluorescence spectrophotometer, respectively. The room-temperature PL QYs of NCs were determined by comparing the integrated emission of the NCs samples in solution with that of a fluorescent dye (rhodamine 6G in ethanol or rhodamine 101 in 0.01% HCl ethanol solution) with identical optical density. Also, the known QYs of the NCs in solution can be used to measure the PL efficiencies of other NCs by comparing their integrated emission. The fluorescence lifetime study was performed by an Edinburgh FL 900 single-photon counting system equipped with a Hamamatsu C8898 ps light pulser. The excitation light was obtained from a 441 nm laser light. The luminescence time range was selected at 0−200 ns. Data were analyzed using a nonlinear least-squares fitting program, with deconvolution of the exciting pulse being ~200 ps. To conduct an investigation by transmission electron microscopy (TEM), the NCs were deposited from dilute toluene solutions onto copper grids with carbon support by slowly evaporating the solvent in air at room temperature. TEM images were acquired using a JEOL JEM-1400 transmission electron microscope operating at an acceleration voltage of 120 kV. Powder X-ray diffraction (XRD) was obtained by wide-angle X-ray scattering using a Siemens D5005 X-ray powder diffractometer equipped with graphite-monochromatized Cu Kα radiation ($\lambda$ = 1.54178 Å). XRD samples were prepared by depositing NCs powder on a piece of Si (100) wafer.

**Photocatalytic Evaluation.** The photocatalytic activity of the as-prepared water-soluble ZCIS/ZnS samples for degradation of RhB in aqueous solution was evaluated by measuring the absorbance of the irradiated solution. Prior to irradiation, 5 mg of ZCIS/ZnS samples was mixed with RhB solution (25 mL, 0.02 mM) in a quartz cell. Then the quartz cell was subsequently illuminated by a 500-W mercury vapor lamp at a 10 cm distance. A wave filter plate ($\lambda$ > 420 nm) was utilized to allow only visible light to transmit. During irradiation, the suspension was vigorously stirred and the reaction temperature was kept at room temperature using a water cooling system. At a given time interval, the dye concentration in the irradiated solution was monitored by measuring the absorption intensity of RhB at 553 nm. The degradation efficiency ($E_{ff}$) was evaluated according to $E_{ff}$ (%) = $(1 - C/C_o) \times 100\%$, where $C_o$ and $C$ represent the absorbance of the dye solution before and after irradiation, respectively.

## RESULT AND DISCUSSION

**Synthesis and Optical Properties of ZCIS NCs.** In recent years, metal carboxylates have been predominantly used as metal

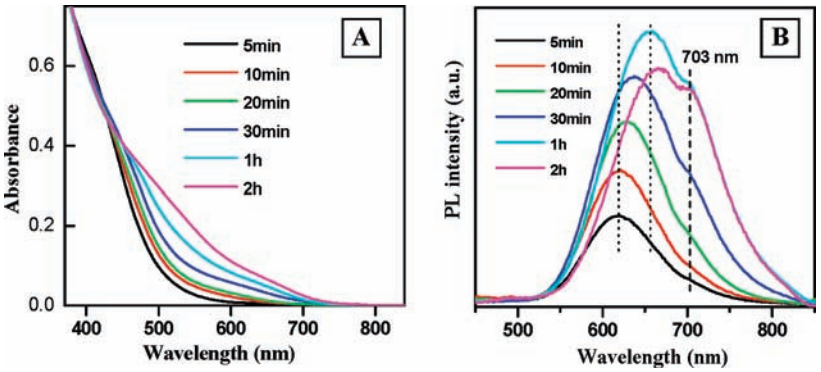


**Figure 1.** Temporal evolution of UV−vis absorption (A) and PL emission spectra (B, $\lambda_{ex}$ = 350 nm) of ZCIS NCs samples in chloroform solution.

cation precursors for the synthesis of semiconductor NCs in organic media because of their stability, convenient availability, relatively low toxicity, and economic nature. An obvious challenge for the synthesis of I−III−VI chalcopyrite semiconductors NCs is their ternary composition. As a result, the stoichiometric ratio between the Group I and the Group III elements of a nanocrystal may vary substantially in a given sample. Due to the higher reactivity of copper fatty acid salts compared with indium fatty acid salts, it has been demonstrated that formation of $Cu_xS$ ($x$ = 1−2) nanophases was almost inevitable when indium and copper carboxylates were used as precursors in the preparation of CIS NCs in the reaction media composed of pure noncoordinating solvent (such as octadecene, ODE), trioctylphosphine oxide (TOPO), amines, carboxylic acid, or their mixtures.[35] The key to successful preparation of alloyed NCs is the ability to tune the relative chemical reactivity of the precursor of constituents to prevent independent nucleation and growth.[7,8] Being a soft Lewis acid, $Cu^{2+}/Cu^{+}$ is of high possibility for the formation of stable complexes with soft Lewis base ligands such as alkyl thiols and thus suppresses substantially the reactivity of Cu precursor. It was noted that alkyl thiols were extensively used as ligands for successful preparation of I−III−VI semiconductor nanocrystals previously.[28,31−33]

The modified literature method was adopted for preparation of ZCIS NCs.[32] ZCIS NCs were prepared in a noncoordinating solvent ODE using acetate salts of Cu, In, and Zn as cation precursor in the presence of steric acid and dodecanethiol. The compound of dodecanethiol serves as the sulfur source and the stabilizing ligand for the formed NCs simultaneously. The temporal evolution of the absorption and emission spectra of ZCIS NCs prepared at a Zn:Cu:In precursor ratio of 1:2:2 at a reaction temperature of 230 °C was shown in Figure 1. For comparison, the plain CIS NCs without the existence of Zn precursor were also synthesized under identical experimental conditions, and the corresponding optical spectra are shown in Figure S1 of the Supporting Information.

The absorption spectra of ZCIS NCs (Figure 1A) were similar to those of typical I−III−VI semiconductor NCs as observed previously in the literature,[21−33,36,37] showing a broad shoulder with a trail in the long-wavelength direction. The first excitonic absorption peaks in the NCs are not as clear as those in binary II−VI QDs.[38,39] The lack of a distinct exciton peak in the absorption spectrum coupled with a long tail on the low-energy side could be the result of several factors alone or in combination with each other. First, it could be indicative of a wide size distribution. Second, it could be a result of electron density leakage from the core of the nanocrystals into the organic ligand layer. Third, it could be the result of intra-band-gap states. This poorly resolved absorption spectrum is characteristic of ternary and quaternary alloyed nanocrystals, which is not caused solely by the wide size distribution since the special electronic properties are considered as one possible reason, and the irregular composition distribution among different NCs in an ensemble can also be one of the reasons.[40] The observed shoulder in the absorption spectra is assigned to the excitonic transition of the ZCIS NCs, which underwent a substantial red shift from 530 to 710 nm during a period of 2 h growth process. In comparison, the corresponding optical band gaps of CIS shifted from 610 to 750 nm under identical reaction conditions. This relative blue shift of the excitonic absorption peak observed in the ZCIS NCs clearly demonstrated incorporation of higher band-gap ZnS into the CIS NCs.[7−9]

The typical PL emission spectrum is wide and composed of two peaks. In the beginning stage (<30 min), the peak in the short wavelength side (referred to the first peak) dominated the spectral profile and the intensity of the peak at the long wavelength side (referred to the second peak) was almost negligible. With prolonging reaction time, both peaks in the spectra profile became stronger and reached the maximum after 1 h growth time but the second peak increased faster and gradually became nearly similar in intensity to the peak at the short wavelength side after 1 h. On the other hand, with extending the heating time, the peak position of the first peak red shifted pronouncedly from 610 to 655 nm in a 1 h period, whereas the second peak showed a fixed wavelength position at 703 nm. It should be pointed out that the peak at 703 nm is not the second harmonic of the excitation wavelength of 350 nm since this peak exists under different excitation wavelengths. If the heating time was too long (>4 h), precipitation of the NCs within the reaction mixture occurred and the corresponding luminescence quenched gradually. Multiple peaks in the PL spectra were observed in the CIS samples in previous literature and also in our CIS samples in the controlled experiment without the presence of zinc (Figure S1 in the Supporting Information).[28,33] It has been demonstrated in earlier reports that a broad size distribution cannot account for the observed broad and multiple peaks in the PL spectra of colloidal CIS or ZCIS NCs.[28,33]

**Influence of Experimental Variables on the Optical Properties of ZCIS Alloy NCs.** The PL properties (PL peak position and PL intensity) of the resulting ZCIS NCs were found to be strongly dependent on the experimental variables such as the Zn:CuIn ratio, the amount of ODE-S and DDT used, and the


dx.doi.org/10.1021/ic102559e |*Inorg. Chem.* 2011, 50, 4065–4072

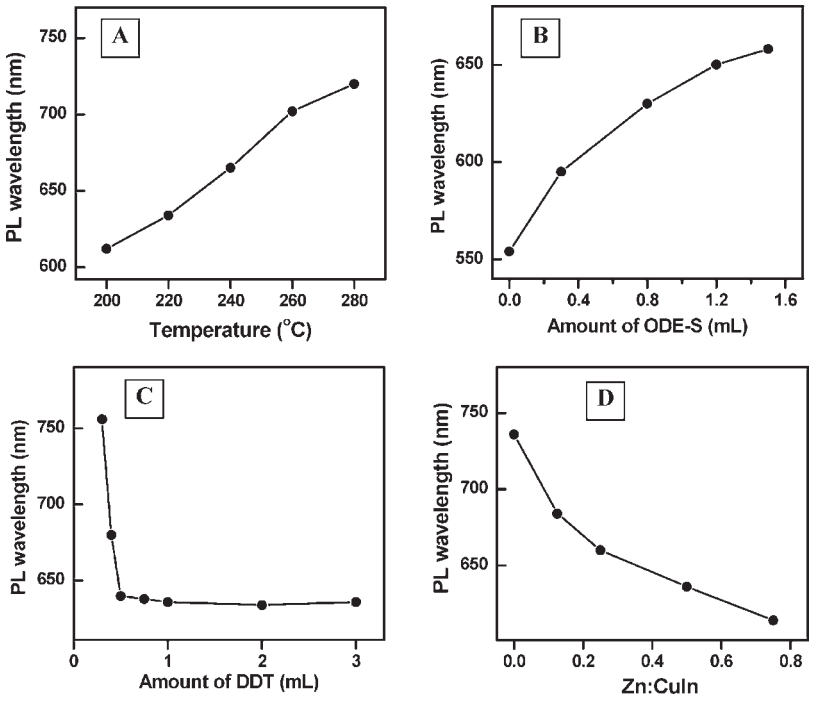


**Figure 2.** Dependence of PL peak position upon different experimental variables with fixation of growth time of 30 min: (A) reaction temperature, (B) Zn:CuIn ratio, (C) amount of ODE-S, and (D) amount of DDT.

reaction temperature. Since the PL QYs of all as-prepared ZCIS NCs under different experimental conditions were not high (usually less than 3%) and cannot approach the desired value for practical application, the PL QYs were not taken into consideration in the investigation of the experimental variables. The improvement of PL QYs was mainly achieved via construction of the ZnS shell around the ZCIS core nanoparticles as discussed below. Hereafter we only described the dependence of PL wavelength on experimental variables. In the investigation of the influence of different experimental variables on the PL wavelength of the obtained ZCIS NCs, we fixed all other experimental variables as stated in the Experimental Section and varied the studied variable only.

**Effect of Reaction Temperature.** The PL peak position of the resulting ZCIS NCs was found to be strongly dependent on the reaction temperature. With an increase of the reaction temperature (200−280 °C) the PL peak position shifted to longer wavelength from 620 to 740 nm systematically (Figure 2A). TEM results indicated that the red-shifted PL peak position derived from the increase of particle size. If reaction temperature was too low (less than 200 °C), no PL emission can be observed, while if reaction temperature was too high (>280 °C) precipitation of the NCs within the reaction mixture occurred. The observed precipitation can be attributed to the fact that DDT acts as both the sulfur precursor and the stabilizing ligand during the reaction. Therefore, its gradual decomposition at too high temperature results in a destabilization of the colloids. Unlike the case of the CIS system reported by Xie et al., where PL emission could be observed for CIS NCs prepared even at 60 °C,[32] in our case low or even no PL emission for samples prepared at low temperature was observed

**Effect of Amount of ODE-S.** With an increase of the amount of ODE-S, the experimental results revealed that the PL peak position red shifted systematically from 550 to 660 nm (Figure 2B). For the red shift of the band gap, usually it can be attributed to the increase of the particle size and/or increase of the relative content of the constituent with a lower band-gap energy. In our case, TEM results show that the particle size under different amounts of ODE-S has no observable difference. This can exclude the reason for the increase of the particle size. In fact, ICP results show that the Cu/In ratio enhanced upon an increase of the amount of ODE-S (data available in Figure S2, Supporting Information). Since the band gap of $Cu_xS$ is lower than that of CIS or ZCIS, the higher Cu/In ratio in the ZCIS system caused a lower band gap.

**Effect of Amount of DDT.** Figure 2C shows that under the fixation of other reaction variables, the PL peak position of the resulting ZCIS was found to be strongly dependent on the amount of thiol, and this dependence can be divided into two ranges. When the amount of thiol was less than 0.5 mL, the PL peak position of the resulting ZCIS shifted to short wavelength pronouncedly with an increase in the amount of thiol. The reason should be ascribed to the composition variation under the presence of a relatively low thiol concentration. However, when the amount of thiol was more than 0.5 mL, the concentration of thiol had almost no effect on the PL peak position.

**Effect of Zn Content.** In the next step, we attempted to tune the PL wavelength of the resulting ZCIS NCs by controlling the Zn/CuIn ratio under fixation of other experimental variables. The Zn:CuIn ratio was achieved by controlling the composition of precursors in the synthetic step. In this study, the molar ratio of Zn to Cu in the raw material solution was varied from 0:1 to 0.7:1 and equimolar Cu and In was used in each case. It should be noted that when the Zn:Cu ratio was increased to higher than 1:1, no PL was observed in the resulting ZCIS NCs and thus the reported highest Zn/Cu ratio was 0.7:1. Figure 2D shows clearly that with an increase of Zn content, the PL band gap of the obtained ZCIS NCs blue shifted from 736 to 614 nm with

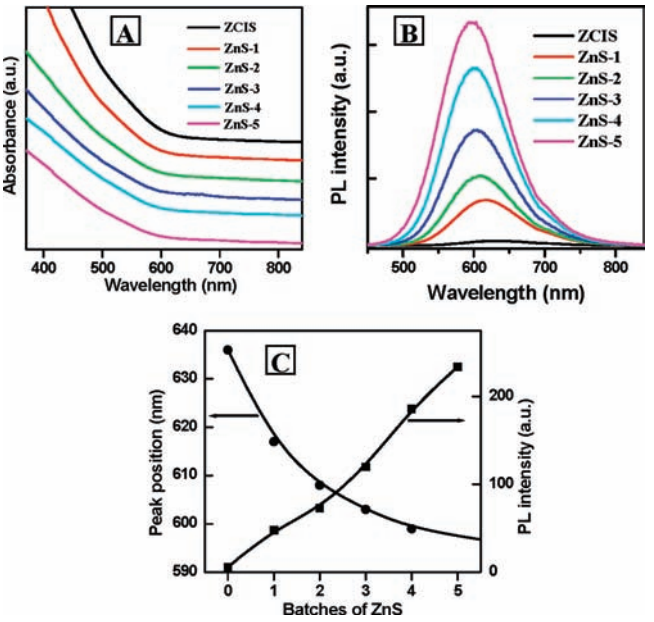


**Figure 3.** Evolution of UV−vis absorption and PL emission spectra ($\lambda_{ex}$ = 430 nm) of the resulting NCs with deposition of the ZnS shell around the ZCIS core NCs.

variation of the Zn:Cu precursor ratio from 0 to 0.75. The increase of the band-gap energy can be ascribed to incorporation of ZnS constituent into the CIS, and thus, $Zn^{2+}$ statistically replaces $Cu^{+}$ and $In^{3+}$. Since the band gap of bulk ZnS (3.6 eV) is substantially higher than that of CuInS (1.5 eV), it is reasonable to observe that the band gap of the alloy of ZnS−$CuInS_2$ is higher than the plain CIS, and this strategy for band-gap tuning has been commonly used in ZnS−CdS and ZnSe−CdSe-alloyed nanostructure systems.[7−10]

**ZCIS/ZnS Core/Shell Structure.** It has been proven that surface passivation of NCs using suitable inorganic materials with a higher band gap is key to improving the PL efficiency and stability of nanocrystals.[41−45] Similar attempts for surface passivation of CIS NCs have appeared in recent literature, and as expected, good optical properties were obtained.[32,33] To improve surface passivation, ZnS comprises a near-ideal candidate for construction of core/shell structure around the ZCIS core based on the following properties: (i) ZnS NCs exhibit relatively chemical stable and nontoxic characteristics under ambient conditions. (ii) The much larger bulk band gap of ZnS ($E_g$ = 3.6 eV) relative to CIS ($E_g$ = 1.5 eV) raises the probability that charge carriers are confined mainly to the CIS core region, resulting in effective "inorganic passivation", in a manner similar to the well-known type-I band alignment the CdSe/ZnS system.[41,42] (iii) The crystal structure of ZCIS can be described as a derivative of the ZnS zinc blende structure in which the zinc positions are occupied by Cu and In, respectively, and the lattice mismatch between CIS and ZnS is relatively low (2−3%), which increases the probability of forming a smooth, low-defect interface between the materials.

The ZCIS/ZnS core/shell structure was constructed in situ from the ZCIS NCs reaction mixture. Due to the large excess of sulfur precursor used in the preparation of ZCIS core NCs, no further sulfur source was added in the process of depositing the ZnS shell. To avoid formation of separate ZnS nanoparticles, Zn precursor ($Zn(OAc)_2$) was added in batches (see details in the Experimental Section). Figure 3 shows the evolution of spectral features of ZCIS/ZnS core/shell NCs starting from the ZCIS cores with a Zn:Cu ratio of 0.5:1. Growth of the ZnS shell improved the emission properties substantially, although it did not affect the absorption spectra significantly (Figure 3A). With formation of ZCIS/ZnS core/shell nanostructure, the PL peak position blue shifted systematically from the original 636 to 596 nm and the corresponding PL intensity increased about 30 times (Figure 3C). The blue shift of the PL peak position in the progress of ZnS indicates further incorporation of the zinc component into the core material, resulting in an increase of the band-gap energy. A similar result was also observed in the CIS/ZnS system in previous literature.[32,33] Before growth of the ZnS shell, the ZCIS plain core NCs did show PL emission but with quite low PL quantum yield (typically below 3%). After ZnS shell growth, the PL properties of the resulting core/shell NCs became quite good. Without substantial optimization, the PL QY increased more than 30 times and the highest PL QY reached to 56%. This QY is among the highest reported values for ternary chalcopyrite NCs to date[18−33] and open the way for the use of ZCIS/ZNS NCs in many applications such as light-emitting devices or fluorescent biological labeling and sensing. It should be noted that the multipeak shape of the PL spectra in the ZCIS core NCs was evolved into a single broad peak after deposition of the ZnS shell. In this studied core/shell structure, since the band gap of the ZCIS core can be conveniently tuned via variation of the Zn/Cu ratio, the band gap (or emission wavelength) of the resulting ZCIS/ZnS core/shell structure can also be tuned through variation of the Zn/Cu ratio in the starting ZCIS core NCs. As shown in Figure 4A and 4B, the emission wavelength of the ZCIS/ZnS NCs starting from ZCIS core NCs with different Zn/Cu ratios can cover most of the visible and near-infrared window (from 518 to 810 nm) with high brightness.

**Water-Soluble NCs.** The as-prepared ZCIS/ZnS NCs not only show high PL QYs in the oil phase but also remain high luminescent when transferred into aqueous media via ligand replacement by MUA. Our experimental results show that the water-soluble ZCIS/ZnS NCs can keep up to 90% of the luminescent intensity of the original oil-soluble NCs (Figure 4C). For visibility, Figure 4D shows the luminescence photographs of two representative ZCIS/ZnS samples with an emission wavelength in the visible light range to demonstrate the highly bright luminescence in both oil media and aqueous media under illumination of natural room light. The high luminescence of ZCIS/ZnS in aqueous media can be retained for several days without observable quenching. This high PL stability of the water-soluble NIR-emitting QDs renders them of special interest in the in vivo imaging application.

**Lifetime of Fluorescence of ZnCuInS/ZnS Core/Shell NCs.** It has been reported that the intrinsic defects, size-dependent band gap, and surface defects of NCs are all involved in the PL emission.[46] Different electron−hole recombination mechanisms may correspond to different PL decay lifetimes. We performed measurements of the decay curves of the PL emission of the ZCIS sample with an emission wavelength of 763 nm (denoted as $ZCIS_{763}$) and the corresponding ZCIS/ZnS core/shell NCs with an emission wavelength of 720 nm (denoted as ZCIS/$ZnS_{720}$) (see Figure 5. In general, the PL decay curve for each sample can be well fitted by a triexponential function

$$I(t) = A_1 \exp(-t/\tau_1) + A_2 \exp(-t/\tau_2) + A_3 \exp(-t/\tau_3)$$

where $\tau_1$ ($\tau_2$, $\tau_3$) represents the decay time of the PL emission and $A_1$ ($A_2$, $A_3$) represents the relative weights of the decay


dx.doi.org/10.1021/ic102559e |Inorg. Chem. 2011, 50, 4065–4072

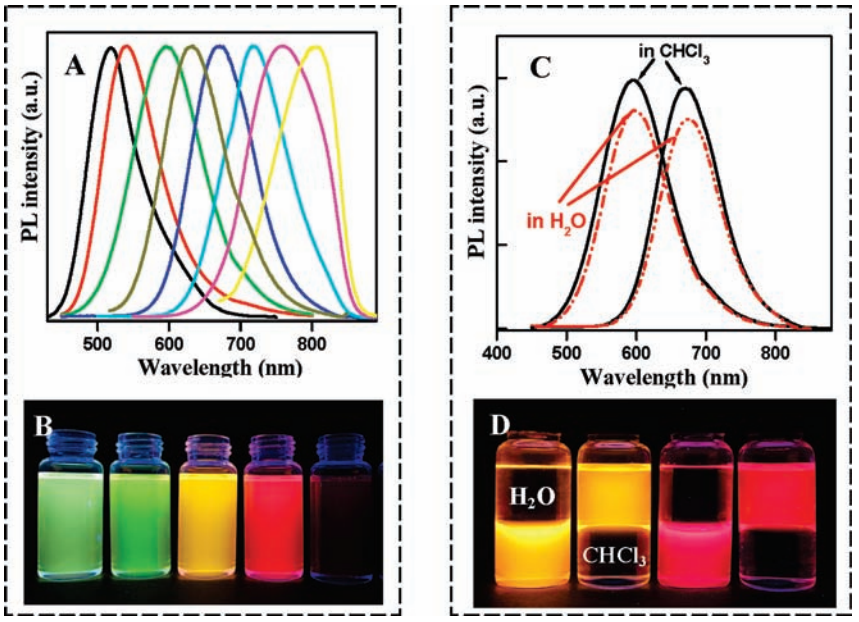


**Figure 4.** Normalized PL spectra ($\lambda_{ex}$ = 360 nm) of NCIS/ZnS core/shell NCs starting from ZCIS core with different Zn/Cu ratios (A), and representative emission colors of NCs dispersion in chloroform under the radiation of a UV lamp (B); comparison of PL spectra of ZCIS/ZnS samples in chloroform and aqueous solutions with identical absorbance at the excitation wavelength (C), and corresponding photographs under illumination of a UV lamp (D).

components at $t = 0$. These constants obtained by the fitting are shown in Table 1, with $\tau_1$ of several nanoseconds, $\tau_2$ ranging from 74.6 to 79.7 ns, and $\tau_3$ ranging from 275 to 385 ns. In previous PL decay investigations of binary II−VI quantum dots (such as CdSe and CdTe),[44,47,48] it has been revealed that the radiative time of binary II−VI QDs has a universal biexponential time distribution. Typically, a shorter lifetime is on the time scale of several nanoseconds, and a longer lifetime is tens of nanoseconds. The shorter lifetime is attributed to the initially populated core-state recombination, while the longer lifetime is due to the surface-related radiative recombination of carriers. In our case, the two radiative lifetimes $\tau_1$ and $\tau_2$ may be assigned to intrinsic recombination of initially populated core states and surface states, respectively. The longest luminescence lifetime (hundreds of nanoseconds) is attributed to donor−acceptor transition, which accounts for a large amount (85−92%) of the total PL emission spectra. This can also explain the broad emission peaks (fwhm of the peaks is ca. 100 nm) of the resulting NCs. In this sense, the time-resolved measurements indicate that there exist three types of PL radiative mechanisms in the PL spectrum of the as-prepared ZCIS and ZCIS/ZnS nanoparticles and the PL emission mainly originates from the intrinsic donor−acceptor transition. It was found that with the overgrowth of the ZnS shell around the ZCIS core NCs the mean PL decay times (i.e., the exciton lifetime $\tau_{1/e}$, at which the PL intensity decreases to 1/e of its initial value) decreased. In addition, the $\tau_3$ values in the ZCIS core samples are larger than those in ZCIS/ZnS core/shell structure samples, and the proportion of the donor−acceptor transition component, related to $A_3$, also became larger in the core samples. This demonstrates the higher weight of donor−acceptor recombination of carriers in the ZCIS core samples.

**Structural Characterization.** Structural characterization was carried out by means of p-XRD. Figure 6 shows the XRD patterns

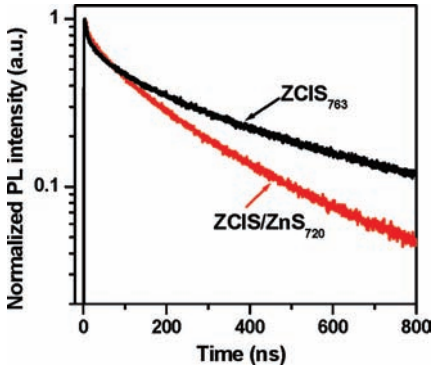


**Figure 5.** Luminescence decay cures ($\lambda_{ex}$ = 441 nm, measured at the maximum of the exciton emission peak) of $ZCIS_{763}$ core NCs and the corresponding $ZCIS/ZnS_{720}$ samples.

**Table 1. Fit Parameters Deriving from $I(t) = A_1 \exp(-t/\tau_1) + A_2 \exp(-t/\tau_2) + A_3 \exp(-t/\tau_3)$**

| samples | $\tau_1$/ns | $A_1$/% | $\tau_2$/ns | $A_2$/% | $\tau_3$/ns | $A_3$/% | lifetime/ns |
|---|---|---|---|---|---|---|---|
| $ZCIS_{763}$ | 10.0 | 0.57 | 74.4 | 7.42 | 385 | 92.01 | 323 |
| $ZCIS/ZnS_{720}$ | 9.8 | 0.51 | 79.7 | 14.4 | 275 | 85.12 | 226 |

for the representative ZCIS core and corresponding ZCIS/ZnS core/shell structure starting from the core. The XRD patterns of both ZCIS and ZCIS/ZnS NCs consist of the characteristic peaks of the zinc blende (cubic) structure. The diffraction peaks are broadened due to the finite particle size. When the ZnS shell deposited around the ZCIS core, the pattern of the cubic lattice is maintained in the core/shell structures but the diffraction peaks shift to larger angles, consistent with the smaller lattice constant for ZnS compared with ZCIS.


dx.doi.org/10.1021/ic102559e |*Inorg. Chem.* 2011, 50, 4065–4072

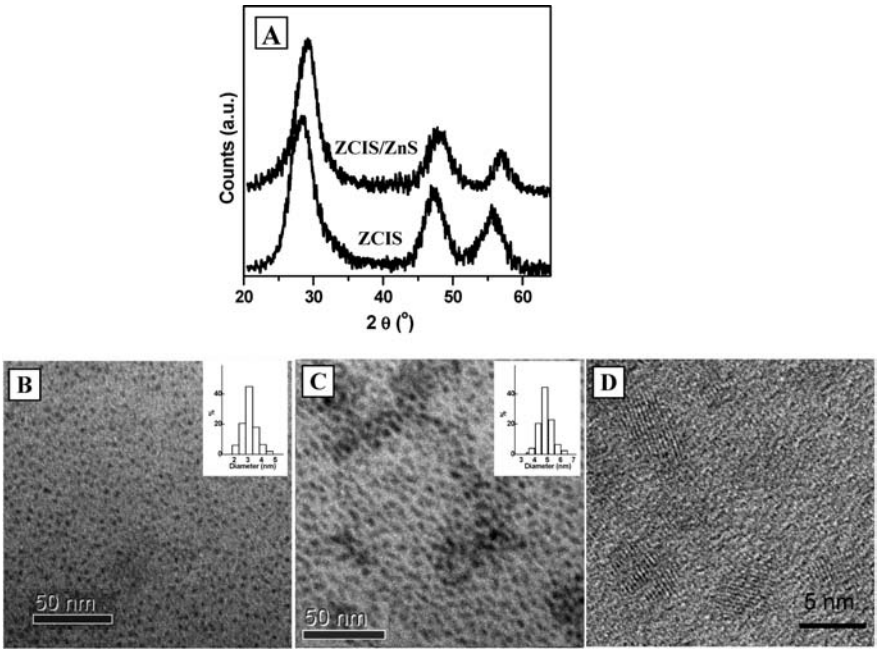


**Figure 6.** (A) XRD patterns of ZCIS and corresponding ZCIS/ZnS NCs. Wide-field TEM images of $ZCIS_{636}$ (B) and corresponding $ZCIS/ZnS_{596}$ core/shell NCs (C). HRTEM image of $ZCIS/ZnS_{596}$ sample (D). (Insets) Corresponding histograms of the size distribution.

Figure 6B−D shows wide-field TEM images of $ZCIS_{636}$ core nanocrystals with an average size of 3.1 nm and the corresponding $ZCIS/ZnS_{596}$ core/shell nanocrystals derived from the initial ZCIS cores via overgrowth of the ZnS shell. The average size of the nearly dot-shaped core/shell nanocrystals in Figure 6C is about 4.8 nm based on the statical analysis of more than 200 particles in a region. All samples of the as-prepared ZCIS and ZCIS/ZnS core/shell nanocrystals have a narrow size distribution with a relative standard deviation ($\sigma$) of 7−10% without any postpreparation fractionation or size sorting, and the corresponding histograms of the size distribution are given as insets of Figure 6B and 6C. As shown in the insets of Figure 6D, the lattice fringes in the HRTEM images of the ZCIS/ZnS core/shell samples run across the entire crystals with no significant contrast variation. Due to the small crystal size and the thin shell thickness, it is almost impossible to observe the ZnS shell around the ZCIS cores by the TEM technique.

**Photocatalytic Activity.** The photocatalytic activity of the as-prepared MUA-capped water-soluble ZCIS/ZnS NCs with an emission wavelength of 600 nm was evaluated for RhB degradation under visible light illumination. The temporal evolution of the UV−vis absorption spectra of the photocatalytic system containing the initial RhB dye concentration of $2 \times 10^{-5}$ M and ZCIS/ZnS NCs catalyst concentration of 0.2 g/L is shown in Figure 7A, and the degradation efficiency (Eff) of the RhB dependent on illumination time is summarized in Figure 7B. It was found that with increasing illumination time, the absorbance of the major absorption peak at 553 nm decreased systematically and the positions of this peak were shifted to shorter wavelength concomitantly, suggesting that the molecular structure of RhB (including both chromophores and aromatic rings) has been destroyed instead of being simply decolorized by adsorption.[49,50] In the first 30 min of illumination, the degradation efficiency was as high as 55% and the RhB was almost decomposed completely within a period of 2 h illumination. To identify the role of NCs in

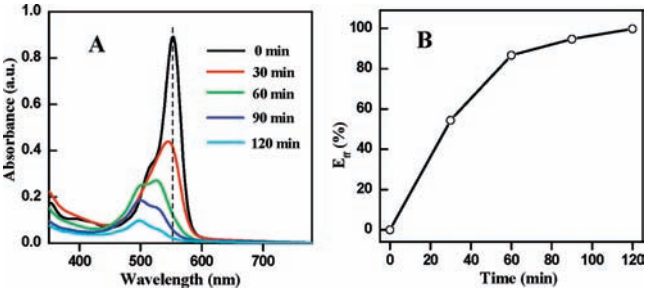


**Figure 7.** Temporal evolution of UV−vis absorption spectra of the photocatalytic degradation system containing RhB ZCIS/ZnS NCs catalyst under visible-light illumination (A), and degradation efficiency (Eff) of RhB dependent on illumination time (B).

the photodegradation of RhB, a blank experiment in the absence of the photocatalyst was investigated under the same conditions. The results show that less than 3% of RhB was degraded after 2 h irradiation, indicating that RhB self-degradation without the photocatalyst could almost be neglected. The corresponding performance of the system containing RHB and capping ligand MUA without ZCIS/ZnS NCs was also carried out, and the results show that MUA have nearly no contribution to the degradation of MO. These experimental results indicate that degradation of the MO should be solely contributed by ZCIS/ZnS NCs.

## CONCLUSIONS

ZCIS-alloyed NCs have been prepared via a "greener" approach in noncoordinating solvent octadecene in the presence of DDT using acetate salts of copper, indium, and zinc as their precursors. The band gap of the ZCIS-alloyed NCs can be conveniently tuned via variation of the stoichiometric ratio of their components. The experimental variables, including the Zn/CuIn ratio, amount of sulfur and dodecanethiol, and reaction


dx.doi.org/10.1021/ic102559e |*Inorg. Chem.* 2011, 50, 4065–4072

temperature, have a significant effect on the band gap of the obtained alloyed NCs. The plain ZCIS NCs did show PL emission but with quite low PL QY (typically below 3%). With the deposition of ZnS shell around the ZCIS core NCs, the PL QY increased substantially with a maximum value of 56% and emission wavelength tunable from 518 to 810 nm. The high PL emission efficiency of the ZCIS/ZnS NCs can also be preserved after phase transfer via ligand replacement. Besides the excellent optical properties, the obtained ZCIS/ZnS NCs also exhibit promising photocatalytical activity in the degradation of rhodamine B.

## ■ ASSOCIATED CONTENT

**Supporting Information.** Absorption and PL spectra of CIS NCs, and the dependence of Cu:In ratio in ZCIS NCs upon the amount of ODE-S.This material is available free of charge via the Internet at http://pubs.acs.org.

## ■ AUTHOR INFORMATION

**Corresponding Author**
*Fax: +86 21 6425 0281. E-mail: zhongxh@ecust.edu.cn.

## ■ ACKNOWLEDGMENT

We thank the National Natural Science Foundation of China (No. 20771037), SRFDP (20070251014), the Fundamental Research Funds for the Central Universities, and the Program for Professor of Special Appointment at Shanghai Institutions of Higher Learning for financial support for financial supports.

## ■ REFERENCES

(1) Peng, X. *Acc. Chem. Res.* **2010**, *43*, 1387.
(2) Somers, R. C.; Bawendi, M. G.; Nocera, D. G. *Chem. Soc. Rev.* **2007**, *36*, 579.
(3) Burda, C.; Chen, X.; Narayanan, R.; El-Sayed, M. A. *Chem. Rev.* **2005**, *105*, 1025.
(4) Panthani, M. G.; Akhavan, V.; Goodfellow, B.; Schmidtke, J. P.; Dunn, L.; Dodabalapur, A.; Barbara, P. F.; Korgel, B. A. *J. Am. Chem. Soc.* **2008**, *130*, 16770.
(5) Tessler, N.; Medvedev, V.; Kazes, M.; Kan, S. H.; Banin, U. *Science* **2002**, *295*, 1506.
(6) Michalet, X.; Pinaud, F. F.; Bentolila, L. A.; Tsay, J. M.; Doose, S.; Li, J.; Sundaresan, G.; Wu, A. *Science* **2005**, *307*, 538.
(7) Zhong, X.; Feng, Y.; Knoll, W.; Han, M. *J. Am. Chem. Soc.* **2003**, *125*, 13559.
(8) Zhong, X.; Han, M.; Dong, Z.; White, T.; Knoll, W. *J. Am. Chem. Soc.* **2003**, *125*, 8589.
(9) Zhong, X.; Feng, Y.; Zhang, Y.; Gu, Z.; Zou, L. *Nanotechnology* **2007**, *18*, 385606.
(10) Zhong, X.; Liu, S.; Zhang, Z.; Li, L.; Wei, Z.; Knoll, W. *J. Mater. Chem.* **2004**, *14*, 2790.
(11) Pan, D.; Wang, X.; Zhou, Z.; Chen, W.; Xu, C.; Lu, Y. *Chem. Mater.* **2009**, *21*, 2489.
(12) Sun, C.; Gardner, J. S.; Long, G.; Bajracharya, C.; Thurber, A.; Punnoose, A.; Rodriguez, R. G.; Pak, J. J. *Chem. Mater.* **2010**, *22*, 2699.
(13) Neumann, B.; Bogdanoff, P.; Tributsch, H. *J. Phys. Chem. C* **2009**, *113*, 20980.
(14) Tang, J.; Hinds, S.; Kelley, S. O.; Sargent, E. H. *Chem. Mater.* **2008**, *20*, 6906.
(15) Uematsu, T.; Taniguchi, S.; Torimoto, T.; Kuwabata, S. *Chem. Commun.* **2009**, *45*, 7485.
(16) Torimoto, T.; Adachi, T.; Okazaki, K-i.; Sakuraoka, M.; Shibayama, T.; Ohtani, B.; Kudo, A.; Kuwabata, S. *J. Am. Chem. Soc.* **2007**, *129*, 12388.
(17) Torimoto, T.; Ogawa, S.; Adachi, T.; Kameyama, T.; Okazaki, K.; Shibayama, T.; Kudo, A.; Kuwabata, S. *Chem. Commun.* **2010**, *46*, 2082.
(18) Nakamura, H.; Kato, W.; Uehara, M.; Nose, K.; Omata, T.; Matsuo, O. S.; Miyazaki, M.; Maeda, H. *Chem. Mater.* **2006**, *18*, 3330.
(19) Pan, D.; Weng, D.; Wang, X.; Xiao, Q.; Chen, W.; Xu, C.; Yang, Z.; Lu, Y. *Chem. Commun.* **2009**, *45*, 4221.
(20) Wang, X.; Pan, D.; Weng, D.; Low, C. Y.; Rice, L.; Han, J.; Lu, Y. *J. Phys. Chem. C* **2010**, *114*, 17293.
(21) Malik, M. A.; O Brien, P.; Revaprasadu, N. *Adv. Mater.* **1999**, *11*, 1441.
(22) Czekelius, C.; Hilgendorff, M.; Spanhel, L.; Bedja, I.; Lerch, M.; Muller, G.; Bloeck, U.; Su, D. S.; Giersig, M. *Adv. Mater.* **1999**, *11*, 643.
(23) Jiang, Y.; Wu, Y.; Mo, X.; Yu, W.; Xie, Y.; Qian, Y. *Inorg. Chem.* **2000**, *39*, 2964.
(24) Lu, Q.; Hu, J.; Tang, K.; Qian, Y.; Zhou, G.; Liu, X. *Inorg. Chem.* **2000**, *39*, 1606.
(25) Xiao, J.; Xie, Y.; Xiong, Y.; Tang, R.; Qian, Y. *J. Mater. Chem.* **2001**, *11*, 1417.
(26) Castro, S. L.; Bailey, S. G.; Banger, K. K.; Hepp, A. F. *Chem. Mater.* **2003**, *15*, 3142.
(27) Arici, E.; Sariciftci, N. S.; Meissner, D. *Adv. Funct. Mater.* **2003**, *13*, 165.
(28) Castro, S. L.; Bailey, S. G.; Banger, K. K.; Hepp, A. F. *J. Phys. Chem. B* **2004**, *108*, 12429.
(29) Nairn, J. J.; Schapiro, P. J.; Twamley, B.; Pounds, T.; Wandruszka, R. V.; Williams, M.; Wang, C.; Notton, M. G. *Nano Lett.* **2006**, *6*, 1218.
(30) Nakamura, H.; Kato, W.; Uehara, M.; Nose, K.; Omata, T.; Matsuo, O. S.; Miyazaki, M.; Maeda, H. *Chem. Mater.* **2006**, *18*, 3330.
(31) Zhong, H.; Zhou, Y.; Ye, M.; He, Y.; Ye, J.; He, C.; Yang, C.; Li, Y. *Chem. Mater.* **2008**, *20*, 6434.
(32) Xie, R.; Rutherford, M.; Peng, X. *J. Am. Chem. Soc.* **2009**, *131*, 5691.
(33) Li, L.; Daou, T. J.; Texier, I.; Chi, T. T. K.; Liem, N. Q.; Reiss, P. *Chem. Mater.* **2009**, *21*, 2422.
(34) Zhang, W.; Chen, G.; Wang, J.; Ye, B.; Zhong, X. *Inorg. Chem.* **2009**, *48*, 9723.
(35) Connor, S, T.; Hsu, C.-M.; Weil, B. D.; Aloni, S.; Cui, Y. *J. Am. Chem. Soc.* **2009**, *131*, 4962.
(36) Kruszynska, M.; Borchert, H.; Parisi, J.; Kolny-Olesiak, J. *J. Am. Chem. Soc.* **2010**, *132*, 15976.
(37) Courtel, F. M.; Hammami, A.; Imbeault, R.; Hersant, G.; Paynter, R. W.; Marsan, B.; Morin, M. *Chem. Mater.* **2010**, *22*, 3752.
(38) Zhong, X.; Feng, Y.; Zhang, Y. *J. Phys. Chem. C* **2007**, *111*, 526.
(39) Qu, L.; Peng, X. *J. Am. Chem. Soc.* **2002**, *124*, 2049.
(40) Greenham, N. C.; Peng, X.; Alivisatos, A. P. *Phys. Rev. B* **1996**, *54*, 17628.
(41) Hines, M. A.; Guyot-Sionnest, P. *J. Phys. Chem.* **1996**, *100*, 468.
(42) Dabbousi, B. O.; Rodriguez-Viejo, J.; Mikulec, F. V.; Heine, J. R.; Mattoussi, H.; Ober, R.; Jensen, K. F.; Bawendi, M. G. *J. Phys. Chem. B* **1997**, *101*, 9463.
(43) Xie, R.; Kolb, U.; Li, J.; Basche, T.; Mews, A. *J. Am. Chem. Soc.* **2005**, *127*, 7480.
(44) Gu, Z.; Zou, L.; Fang, Z.; Zhu, W.; Zhong, X. *Nanotechnology* **2008**, *19*, 135604.
(45) Wang, J.; Long, Y.; Zhang, Y.; Zhong, X.; Zhu, L. *ChemPhysChem* **2009**, *10*, 680.
(46) Zhang, J. Z. *Acc. Chem. Res.* **1997**, *30*, 423.
(47) Li, J. J.; Wang, Y. A.; Guo, W. Z.; Keay, J. C.; Mishima, T. D.; Hohnson, M. B.; Peng, X. G. *J. Am. Chem. Soc.* **2003**, *125*, 12567.
(48) Cumberland, S. L.; Hanif, K. M.; Javier, A.; Khitrov, G. A.; Wowssner, S. M.; Yun, C. S. *Chem. Mater.* **2002**, *14*, 1576.
(49) Li, X.; Kikugawa, N.; Ye, J. *Chem.—Eur. J.* **2009**, *15*, 3538.
(50) Li, X.; Kikugawa, N.; Ye, J. *Adv. Mater.* **2008**, *20*, 3816.